Dalton Transactions

Preparation of magnetic core–shell iron oxide@silica@nickel-ethylene glycol microspheres for highly efficient sorption of uranium (VI)

Journal:	*Dalton Transactions*
Manuscript ID:	DT-ART-12-2014-004040.R1
Article Type:	Paper
Date Submitted by the Author:	25-Jan-2015

Complete List of Authors:	Tan, Lichao; Harbin Engineering University, Key Laboratory of Superlight Material and Surface Technology Zhang, Xiaofei; Harbin Engineering University, Liu, Qi; Harbin Engineering University, Wang, Jun; Harbin Engineering University, School of Material Science and Chemical Engineering Sun, Yanbo; Jilin University, State Key Laboratory of Theoretical and Computational Chemistry, Institute of Theoretical Chemistry jing, xiaoyan liu, jingyuan; harbin engineering university, college of material science and chemical engineering Song, Dalei; Harbin Engineering University, School of Material Science and Chemical Engineering Liu, Lianhe; Harbin Engineering University,

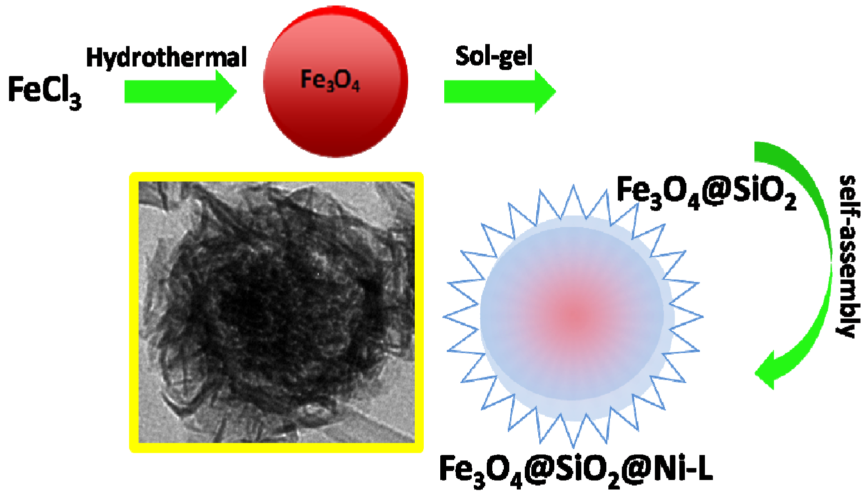
FeCl3
Hydrothermal
Fe3O4
Sol-gel
Fe3O4@SiO2
self-assembly
Fe3O4@SiO2@Ni-L

Cite this: DOI: 10.1039/c0xx00000x

www.rsc.org/xxxxxx

PAPER

Preparation of magnetic core–shell iron oxide@silica@nickel-ethylene glycol microspheres for highly efficient sorption of uranium (VI)

Lichao Tan,[a] Xiaofei Zhang,[a,d] Qi Liu,*[a] Jun Wang,*[a, b] Yanbo Sun,[c] Xiaoyan Jing,[a] Jingyuan Liu,[a] Dalei Song,[a] and Lianhe Liu[b]

Received (in XXX, XXX) Xth XXXXXXXXX 20XX, Accepted Xth XXXXXXXXX 20XX
DOI: 10.1039/b000000x

We report a facile approach for the formation of magnetic core–shell iron oxide@silica@nickel-ethylene glycol (Fe_3O_4@SiO_2@Ni-L) microspheres. The structure and morphology of Fe_3O_4@SiO_2@Ni-L are characterized by X-ray diffraction (XRD), scanning electron microscopy (SEM), transmission electron microscopy (TEM) and nitrogen sorption isotherm. The composite possesses high specific surface area of 382 m^2 g^{-1}. The obtained core/shell structure is composed of a superparamagnetic core with a strong response to external fields, which are recovered readily from aqueous solution by magnetic separation. When used as the adsorbent for uranium (VI) in water, the as-prepared Fe_3O_4@SiO_2@Ni-L multi-structural microspheres exhibit a high adsorption capacity, which is mainly attributed to the large specific surface area and typical mesoporous characteristics of Fe_3O_4@SiO_2@Ni-L microspheres. This work provides a promising approach for the design and synthesis of multifunctional microspheres, which can be used for water treatment, as well as having other potential applications in a variety of biomedical fields including drug delivery and biosensors.

Introduction

With the rapid development of nuclear power and nuclear techniques, the environment faces more and more contamination than in the past. Uranium mining and hydrometallurgy produce a large quantity of uranium waste water, which causes a serious threat to the ecological environment and waste resources.[1, 2] Hence, it is very important to remove uranium from water. The most used methods for separation of uranium from aqueous waste streams include chemical precipitation, electrolysis, chromatographic extraction, solvent extraction, ion exchange and adsorption.[3-6] Compared with other methods, adsorption is efficient and easy to operate, which is widely used for wastewater treatment process.[7] As a desirable approach, adsorption processes are widely used in water treatment. Developing novel sorbents is presenting significant opportunities to improve the nuclear fuel cycle.[8, 9]

Nickel-based materials have an important function, and are employed in various fields, such as batteries,[10] optics,[11] gas-sensing devices,[12] electrochemical capacitors,[13] and catalysis.[14] materials with hierarchical nanostructures.[15-16] Elabd et al. reported that, hydroxides of nickel can be employed as an adsorbent. Also, it was reported that hydrated UO_2^{2+} adsorbed effectively on top of a surface nickel atom through surface complexation with Ni-O bonds.[17] This means that the loading amount of functional groups increases significantly. Moreover, ethylene glycol have more functional groups and easy to combine with nickel. For this reason, Nickel-based materials are expected that the new sorbent materials will show high adsorption capacity for UO_2^{2+}. Unfortunately, it is usually a kind of superfine powder, which is easy to lose in the processes of adsorption and difficult to separate from aqueous systems after batch adsorption experiments.[18]

Certainly, magnetic adsorbents have emerged as a new generation of materials for environmental decontamination since magnetic separation simply involves applying an external magnetic field to remove and recycle the adsorbents. Magnetic composite materials can possibly resolve the above problem. Such materials combine the advantages of activity of adsorbents with the merits of an easy separation by incorporation of magnetic nanoparticles. Magnetite (Fe_3O_4), a common ferrite possessing a cubic, inverse spinel structure, has been widely studied because of its potential application as ferrofluids, catalysts, biological assays, chemical sensors, and electrophotographic developers.[19] With respect to these properties, the design and synthesis of various core/shell architectures based on Fe_3O_4 are important research areas of interest. For instance, Lv et al. prepared magnetic γ-Fe_2O_3@Ti-tmSiO_2 which has been applied in the adsorption of dye.[20] Chitosan-coated Fe_3O_4 nanoparticles showed marked ability in extracting Cu (II).[21] Core-shell structured magnetic material is a kind of novel adsorption material. It can make up the disadvantages of individual adsorption material and improve the adsorption performance. Moreover, it can simplify the regeneration steps and easy to recycle adsorbent.

In this paper we report the synthesis of core–shell structured material with magnetic components encapsulated in Ni-L to enhance the separation and recovery of shell material. The as-obtained Fe_3O_4@SiO_2@Ni-L materials were used as adsorbent in waste-water treatment, and showed an excellent ability to remove uranium (VI) from aqueous solutions.

Experimental

Material Preparation

Fe_3O_4 particles were fabricated by a simple hydrothermal method according to Ref.[22] with a little modification: $FeCl_3·6H_2O$ (2.7 g, 10 mmol) was dissolved in ethylene glycol (80 mL) to form a clear solution, and then NaAc (4.0 g) was added to the solution at 50 °C under vigorous stirring for 30 min. The mixture was then transferred to a Teflon-lined stainless-steel autoclave (100 mL) and heated at 198 °C for 8 h.

The core−shell Fe_3O_4@SiO_2 microspheres were prepared by a sol-gel method as follows.[23] The magnetite particles were dispersed in a mixture of ethanol (280 mL), deionized water (70 mL), and concentrated ammonia aqueous solution (5.0 mL, 28 wt %). After mechanical stirring for 15 min at 30 °C, 4.0 mL of tetraethyl orthosilicate (TEOS) was added dropwise in 2 min. After stirring for 8 h, the Fe_3O_4@SiO_2 microspheres were separated and collected with a magnet, washed with ethanol, and then dried in vacuum at 60 °C for 6 h.

2.328 g of $Ni(NO_3)_2·6H_2O$ and 0.936 g of NaCl were dissolved in 80 mL of ethylene glycol and stirred for 5 min, and then Fe_3O_4@SiO_2 was added and the mixture was ultrasonically dispersed for 15 min. Afterward, 10.496 g of NaAc was added to the above system. After vigorous stirring for 20 min, the mixture was transferred into a Teflon-lined autoclave, heated to 190 °C for 8 h, and finally cooled to room temperature. The precipitate was separated by a magnet, washed with deionized water and ethanol, and dried in air at 60 °C for 24 h.

Adsorption of uranium (VI)

In a typical experiment, 0.05 g of Fe_3O_4@SiO_2@Ni-L microspheres was mixed with 50 mL of $UO_2(NO_3)_2·6H_2O$ solution. After the adsorption processes, the samples were isolated from the supernatant by use of a magnet, and the supernatant solutions were analyzed with WGJ–III Trace Uranium Analyzer to obtain the concentrations of uranium (VI) in solution. The solution pH was adjusted by addition of 0.5 mol L^{-1} HNO_3 and NaOH. The amount of uranium (VI) adsorbed per unit mass of the adsorbent was calculated according to Eq. (1):

$$Q_e = \frac{(C_0 - C_e)V}{m} \qquad (1)$$

where Q_e is the adsorption capacity of adsorbent, C_0 and C_e (mg L^{-1}) are concentration of uranium (VI) at the initial and equilibrium states, respectively, V (L) is the volume of the solution and m is the weight of sorbent (g).

Desorption studies

To investigate the reusability of Fe_3O_4@SiO_2@Ni-L, 0.05 g of Fe_3O_4@SiO_2@Ni-L was first put in contact with 50 mL uranium (VI) for 300 min. After adsorption, desorption was carried out by washing the adsorbents with distilled water several times, and then the solution containing 50 mL of desorptive solutions was added into the adsorbed uranium (VI) adsorbents for 300 min. Before the second adsorption, the adsorbent was treated by 0.1 mol L^{-1} $NaHCO_3$ solution for 300 min. The solid and liquid phases were separated by a magnet. The above procedure was repeated three times to test the reusability of the Fe_3O_4@SiO_2@Ni-L.

Characterization

Crystallite structures were determined by X-ray diffraction (XRD) using a Rigaku D/max-IIIB diffractometer with Cu Kα irradiation (λ = 1.54178 Å). The X-ray source was operated at 40 kV and 150 mA. Fourier-transform infrared (FT-IR) spectrum was recorded with an AVATAR 360 FT-IR spectrophotometer using a standard KBr pellets. The morphology was characterized using transmission electron microscopy (TEM, FEI Tecnai G^2 20 S–TWIN) and a scanning electron microscope (SEM, JSM-6480A, Japan Electronics), equipped with an energy dispersive X-ray spectrometry analyzer (EDS, INC250, Japan Electronic). Nitrogen sorption isotherm was measured at 77 K with TriStar II 3020 Version 2.00 equipment. The magnetic measurement was carried out with a vibrating sample magnetometer (VSM, Lanzhou University LakeShore 7304). Effluent was analyzed using WGJ–III Trace Uranium Analyzer from the Company of Hangzhou Daji Photoelectric Instrument.

Results and discussion

Characterization of samples

The crystal phases of Fe_3O_4, Fe_3O_4@SiO_2 and Fe_3O_4@SiO_2@Ni-L are revealed by the XRD patterns (Fig. 1A), which show that the curve of diffraction peaks marked Fe_3O_4 of (220), (311), (400), (422), (511) and (440) crystal, and the diffraction peaks of Fe_3O_4, can be indexed to cubic Fe_3O_4 (JCPDS: 19-629). After forming complexes Fe_3O_4, SiO_2 and Ni-L, we can see that the broad band around 2θ angle of 22°can be ascribed to amorphous silica.[24] Those obviously broader and weaker peaks most likely indicate the crystalline loss from Fe_3O_4. However, we can see that the crystal of Fe_3O_4 (400) still remain. Moreover, we observe that a strong diffraction peak appears at around 6.2°, which is characteristic of coordination polymers from metal ions and ethylene glycol. [25-27] The following FT-IR and EDS study can provide evidence for this analysis.

For the SEM image of Fe_3O_4 particles, the Fe_3O_4 particles exhibit a spherical morphology and uniform size (Fig. 1B). The SEM image of Fe_3O_4@SiO_2 particles (Fig. 1C) show that after the sol-gel process, which forms a smooth layer of SiO_2 on Fe_3O_4, the product is still spherical; the Fe_3O_4@SiO_2 particles slightly increase in diameter due to accumulation of SiO_2 layers Subsequently, a layer of Ni-L coats on the surface of Fe_3O_4@SiO_2 (Fig. 1D), in which Ni-L is composed of many thin slices of self-assembled units, which uniformly coat around the Fe_3O_4@SiO_2. The Fe_3O_4@SiO_2@Ni-L of EDS spectra is shown in Fig. 1E. The EDS spectra revealed the presence of the elements C, O, Si, Fe and Ni for Fe_3O_4@SiO_2@Ni-L, showing that, the Ni-L particles were distributed onto the surface of Fe_3O_4@SiO_2@Ni-L. To further investigate their microstructure, elemental mapping is employed to investigate the elemental distributions in the core–shell structure, as depicted in Fig. 2. The Fe element stays in the core region, and the Ni and Si elements are detected in the shell region, while the O element can be observed in both regions.

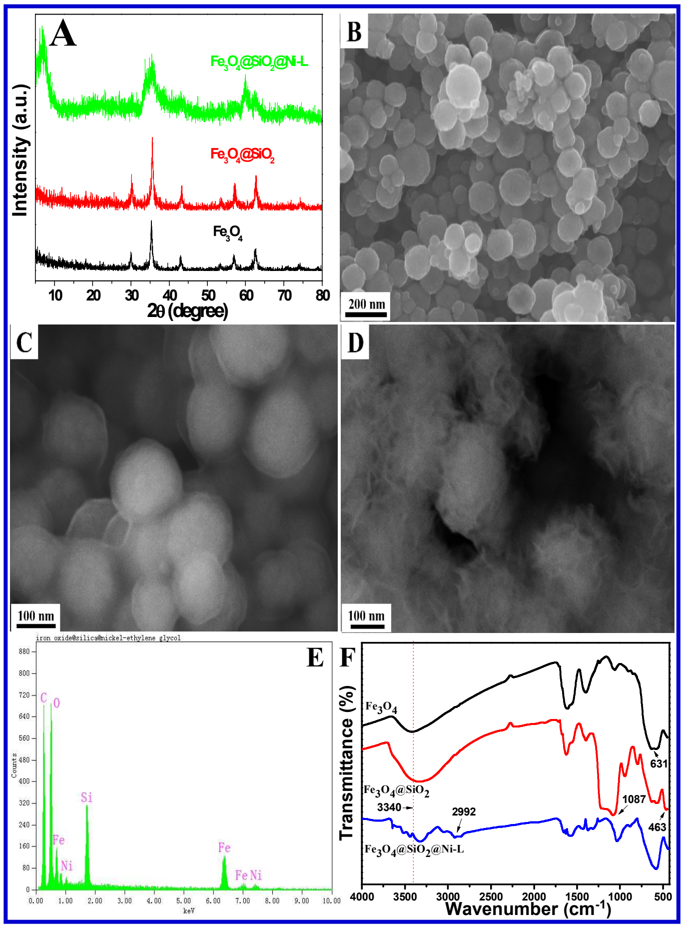

Fig. 1. XRD patterns (A); SEM images of Fe_3O_4 particles (B), $Fe_3O_4@SiO_2$ (C) and $Fe_3O_4@SiO_2@$Ni-L (D); $Fe_3O_4@SiO_2@$Ni-L of EDS spectra (E); FT-IR spectra of Fe_3O_4, $Fe_3O_4@SiO_2$ and $Fe_3O_4@SiO_2@$Ni-L (F).

The TEM image in Fig. 3A clearly shows that the obtained Fe_3O_4 particles are spherical-shaped and have a mean diameter of ~130 nm. After the sol-gel process, core−shell $Fe_3O_4@SiO_2$ microspheres were obtained (Fig. 3B). By a solvothermal procedure, core-shell structured microspheres are formed. The TEM image (Fig. 3C and 3D) of the resulting $Fe_3O_4@SiO_2@$Ni-L microspheres shows that Ni-L nanoplatelets grow/attach to the solid core so that the external surface of the microspheres is composed of platelet edges.

In order to identify the modification with Ni-L functional groups, FT-IR spectra of Fe_3O_4, $Fe_3O_4@SiO_2$ and $Fe_3O_4@SiO_2@$Ni-L were recorded and are shown in Fig. 1F. The peak at 631 cm^{-1} is attributed to the stretching vibration of the Fe-O bond (Fe_3O_4). The broad band around 1087 cm^{-1} is relevant to Si-O-Si and Si-O-H stretching vibrations, and the band around 463 cm^{-1} corresponds to the bending vibration of O-Si-O,[28] reflecting the coating of silica on the magnetite surface ($Fe_3O_4@SiO_2$). After modification with Ni-L ($Fe_3O_4@SiO_2@$Ni-L), the appearance of new band at 2992 cm^{-1} corresponds to C-H stretching vibration. All of materials have the peak at 3340 cm^{-1} which is attributed to the stretching vibration of the O-H bond. Additionally, the $Fe_3O_4@SiO_2@$Ni-L of EDS also is consistent with the FT-IR characterization.

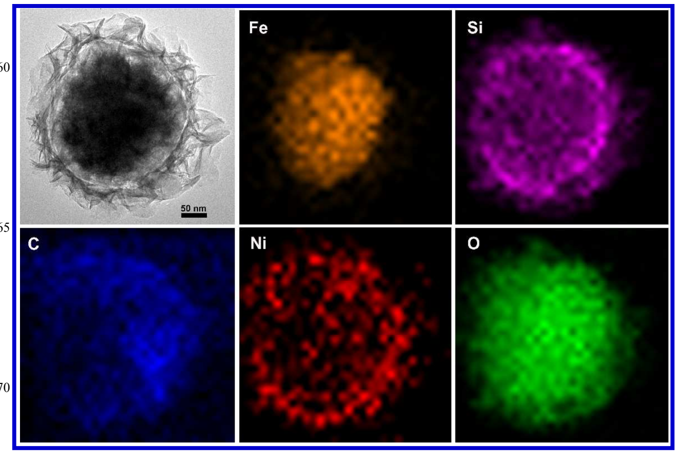

Fig. 2. The elemental mapping shows homogenous dispersion of Fe, Si, C, Ni and O element in the $Fe_3O_4@SiO_2@$Ni-L core-cell microspheres.

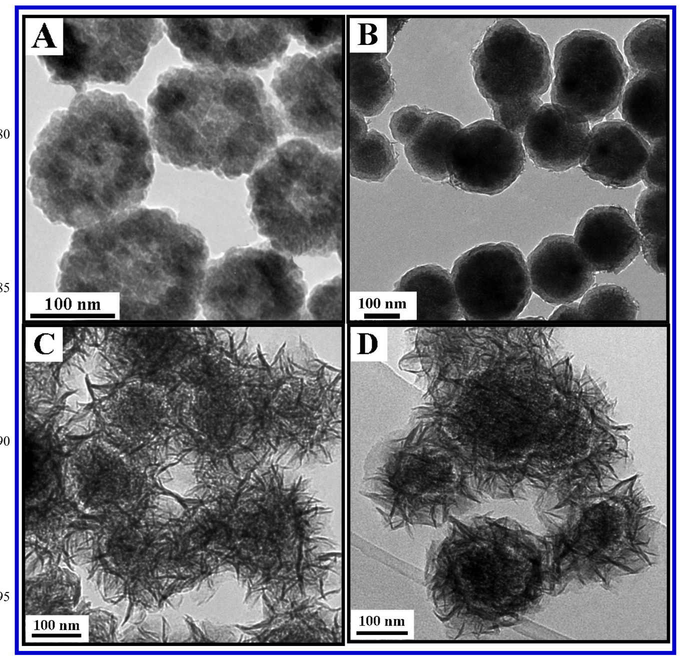

Fig. 3. TEM images of Fe_3O_4 particles (A), $Fe_3O_4@SiO_2$ (B) and $Fe_3O_4@SiO_2@$Ni-L(C, D).

Nitrogen adsorption−desorption analysis was carried out to characterize the specific surface area and porosity of the as-prepared $Fe_3O_4@SiO_2@$Ni-L microspheres. Fig. 4A shows the N_2 adsorption−desorption isotherm, and Fig. 4B shows the BJH pore size distributions of as-synthesized $Fe_3O_4@SiO_2@$Ni-L. We see that both curves exhibit typical IV isotherms with an H3-type hysteresis loop (P/P_0 >0.4), indicating the presence of mesoporous structure in the microspheres. The specific surface area of $Fe_3O_4@SiO_2@$Ni-L is 382 m^2 g^{-1} and the average pore diameter is calculated to be 5.6 nm. As widely reported, a high surface area usually gives rise to high adsorption capacity for an adsorbent in water treatment because of more available active adsorption sites.[29] The hierarchical and mesoporous structures are beneficial to improve the removal efficiency of absorbate molecules.[30-31]

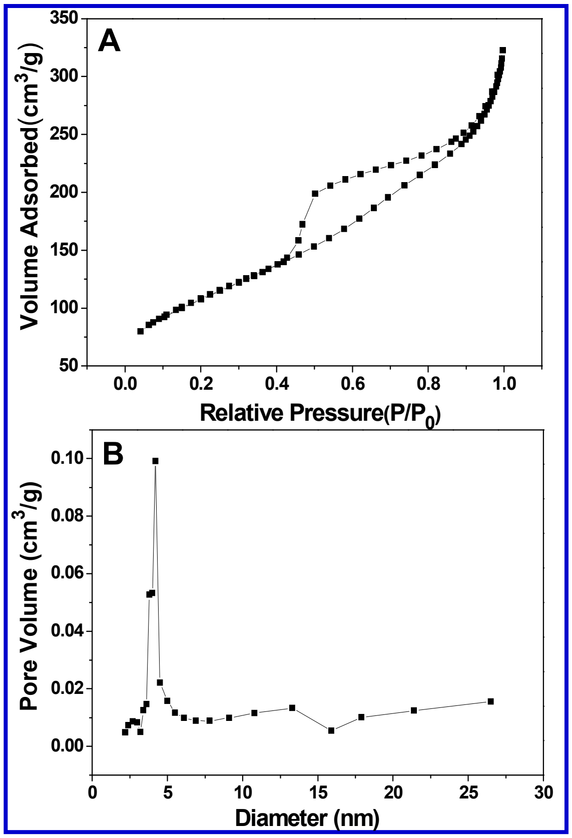

Fig. 4. Nitrogen adsorption-desorption isotherm (A) and pore size distribution plot (B) of $Fe_3O_4@SiO_2@Ni$-L

The magnetic properties of samples were investigated using a VSM. The magnetic hysteresis loops measured at 300 K are illustrated in Fig. 5. The magnetization curves show no remanence or coercivity, suggesting a superparamagnetic character. The saturation magnetizations of Fe_3O_4, $Fe_3O_4@SiO_2$ and $Fe_3O_4@SiO_2@Ni$-L are 86.8, 44.3 and 20.9 emu g^{-1}, respectively. Although the saturation magnetization decreases, the saturation magnetization is enough to enable the manipulation of $Fe_3O_4@SiO_2@Ni$-L by conventional magnets. The results reveal that the particles exhibit a desirable magnetic response, suggesting a potential application as adsorbents.

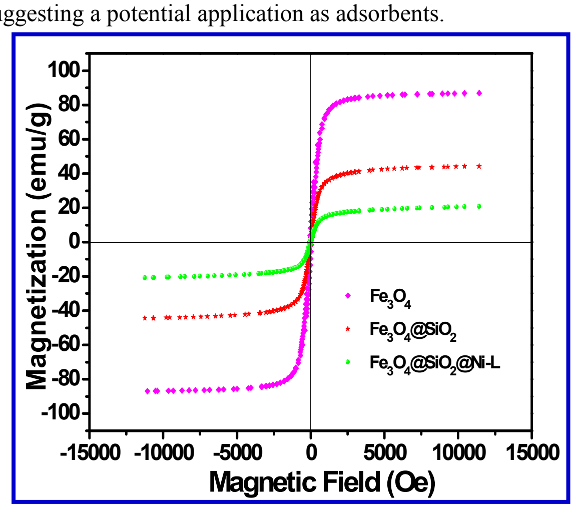

Fig. 5. Magnetic hysteresis loop for Fe_3O_4, $Fe_3O_4@SiO_2$ and $Fe_3O_4@SiO_2@Ni$-L at 300 K.

Effect of pH on the uranium (VI) adsorption

Solution pH is one of the most important variables affecting the adsorption characteristics. Adsorption of uranium (VI) on as function of pH value is shown in Fig. 6. It is clear that uranium (VI) adsorption on $Fe_3O_4@SiO_2@Ni$-L is strongly dependent on pH value. As pH increases from 2.0 to 5.0, the adsorption capacity of uranium (VI) on $Fe_3O_4@SiO_2@Ni$-L increases. The maximum adsorption capacity occurs at pH 5.0. The adsorption capacity diminishes as pH continues to rise from 5.0 to 12.0. At lower pH, the predominant uranium species is UO_2^{2+} ion and its adsorption on $Fe_3O_4@SiO_2@Ni$-L is reduced due to the availability of a limited number of complexing sites as well as electrostatic repulsion of protonated active sites. The uranium adsorption on $Fe_3O_4@SiO_2@Ni$-L is observed to be maximum at pH 5.0, and the amount of uranium adsorbed is determined to be 129.26 mg U/g at pH 5.0. With a pH higher than 5.0, uranium is present in the anionic form by complexation with carbonate and hydroxyl anions which has less interaction with functional groups of $Fe_3O_4@SiO_2@Ni$-L leading to a decrease in adsorption.[32-33] Consequently, pH 5.0 is considered as the optimum pH for further experiments.

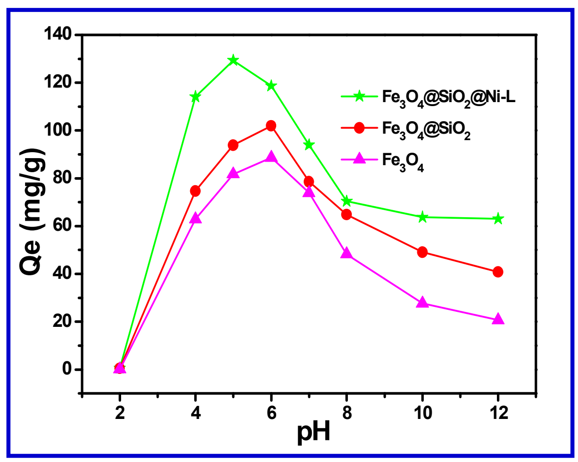

Fig. 6. Effect of initial pH on adsorption of uranium by Fe_3O_4, $Fe_3O_4@SiO_2$ and $Fe_3O_4@SiO_2@Ni$-L. (Adsorption dosage 0.05 g, retention time 300 min, T = 25 °C and pH = 2 ~ 12).

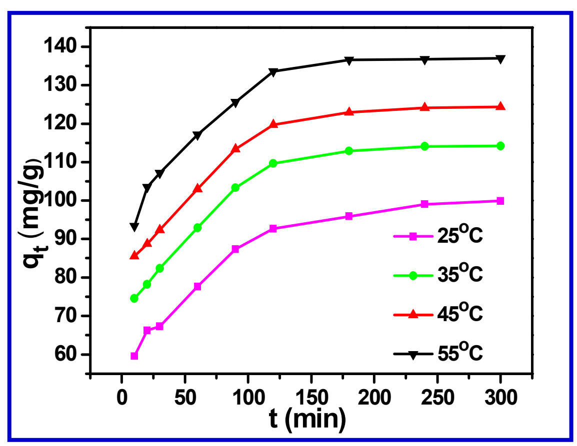

Fig. 7. Effect of reaction time on the adsorption of uranium by $Fe_3O_4@SiO_2@Ni$-L. (Adsorption dosage 0.05 g reaction time 5 min ~ 300 min, T = 25 ~ 55 °C and pH = 5).

The adsorption of uranium (VI) onto Fe_3O_4, Fe_3O_4@SiO_2 and Fe_3O_4@SiO_2@Ni-L was carried out by varying pH in the range of 2.0−12.0 (Fig. 6). Fe_3O_4 and Fe_3O_4@SiO_2 show low adsorption capacity for uranium, indicating that Fe_3O_4 and Fe_3O_4@SiO_2 have a rare contribution for uranium removal in the composite. In contrast, Fe_3O_4@SiO_2@Ni-L has high adsorption capacity for uranium, meaning that Ni-L mostly contribute to uranium removal in the composite. Fe_3O_4@SiO_2@Ni-L shows high adsorption capacity for uranium, indicating this uniquely structured composite are favorable for achieving high adsorption performance.

Effect of contact time on uranium sorption

The effect of contact time on the adsorption of uranium (VI) onto Fe_3O_4@SiO_2@Ni-L was studied under a constant concentration of uranium solution at 298-328 K. It was observed that adsorption of uranium was rapid in the first 120 min and then gradually attained an equilibrium within 240 min, suggesting strong chemisorptions or surface complexation of uranium with Fe_3O_4@SiO_2@Ni-L (Fig. 7). The fast sorption kinetics indicates that Fe_3O_4@SiO_2@Ni-L may have good potentialities for real application in adsorbing uranium (VI) from large volumes of aqueous solutions. Based on the kinetic data, 300 min was selected to ensure the equilibrium of uranium (VI) sorption on Fe_3O_4@SiO_2@Ni-L in the following experiments.

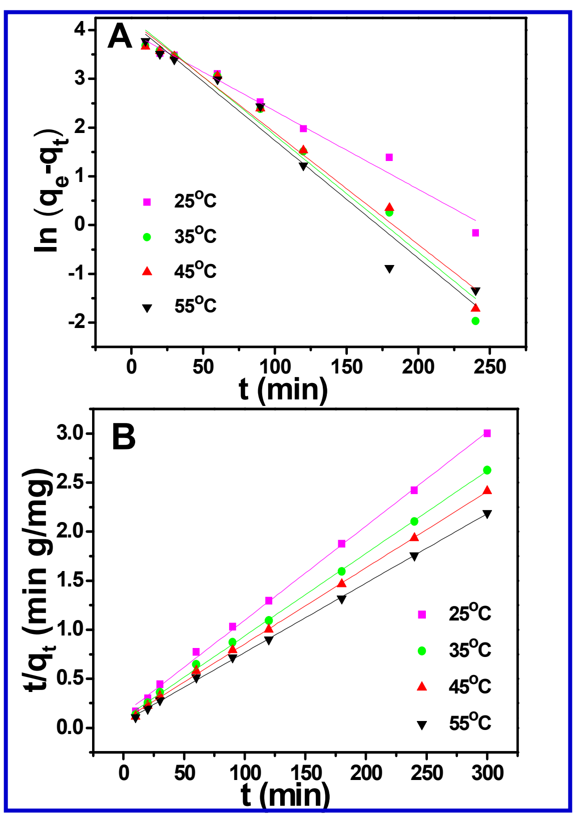

Fig. 8. Pseudo-first-order kinetics and Pseudo-second-order kinetics for removal of uranium by Fe_3O_4@SiO_2@Ni-L.

Adsorption kinetics

The kinetics of adsorption was studied to investigate the mechanism of adsorption, and the pseudo-first-order and pseudo-second-order models were tested to fit experimental data of uranium adsorption on Fe_3O_4@SiO_2@Ni-L (Fig. 8). The pseudo-first-order model [34] can be expressed by:

$$\ln\left(q_e - q_t\right) = \ln q_e - k_1 t \quad (2)$$

where q_e and q_t (mg g^{-1}) are the adsorption capacity of uranium (VI) at equilibrium and at various times t, respectively, and k_1 (1/h) is the rate constant of the pseudo first-order model. The values of q_e and k_1 are determined from the intercept and slope of the linear plot of $\ln(q_e - q_t)$ versus t.

The pseudo second-order model [35] is represented by:

$$t/q_t = 1/k_2 \cdot q_e^2 + t/q_e \quad (3)$$

where k_2 (g mg^{-1} h^{-1}) is the pseudo-second-order adsorption rate constant. The values of q_e and k_2 are obtained from the slope and intercept of the plots of t/q_t against t. The calculated kinetic parameters from both model fittings are shown in Table 1. Obviously, the correlation coefficient (R^2) of the pseudo-second-order model is higher than that of the pseudo-first-order model. Moreover, the $q_{e,cal}$ value for the pseudo-second-order model is closer to the experimental value ($q_{e,exp}$). These results suggest that a pseudo-second-order sorption is the predominant mechanism. These results suggest that a pseudo-second-order sorption is the predominant mechanism and the rate constant of uranium (VI) appears to be controlled by the chemisorption process. It is also indicated that the rate-determining step might be chemical adsorption and the adsorption behavior might involve the valency forces through sharing electrons between uranium (VI) ions and adsorbents.[36-37]

Table 1 Kinetic parameters for adsorption of uranium on Fe_3O_4@SiO_2@Ni-L.

Kinetic models and parameters	25 °C	35 °C	45 °C	55 °C
Pseudo-first-order				
$q_{e,cal}$ (mg L^{-1})	51.72	69.53	66.13	63.78
k_1 (min^{-1})	0.0161	0.0239	0.0230	0.0242
R^2	0.98	0.97	0.98	0.96
Pseudo-second-order				
$q_{e,cal}$ (mg L^{-1})	104.17	118.76	128.70	141.24
k_2 (g mg^{-1} min^{-1})	0.000687	0.000749	0.000777	0.000843
R^2	0.99	0.99	0.99	0.99

Effect of temperature and adsorption thermodynamics

Adsorption isotherm models are usually used to describe the interaction between the adsorbent and the adsorbate when the adsorption process reaches equilibrium, affording the most important parameter for designing a desired adsorption system. The effect of temperature on the adsorption of uranium on Fe_3O_4@SiO_2@Ni-L particles was studied in the range of 298–328 K (Fig. 9). It is obvious that most sorption occurs at 328 K and least at 298 K, indicating that high temperature is advantageous for uranium (VI) sorption. The thermodynamic parameters (*ΔH*°, *ΔS*° and *ΔG*°) are calculated from the temperature dependence of sorption isotherms (Fig. 10). The adsorption standard Gibbs free energy changes (*ΔG*°) can be calculated as follows:

$$\Delta G^0 = -RT \ln K_d \quad (4)$$

where R is the gas constant (8.314 J mol^{-1} K^{-1}) and T is the temperature in Kelvin. The average standard enthalpy change (*ΔH*°) is obtained from the Van't Hoff equation:

$$\ln K_d = -\Delta H^0 / RT + \Delta S^0 / R \quad (5)$$

where K_d is the distribution coefficient (mL g^{-1}) of uranium (VI), T is absolute temperature (K), and R is the ideal gas constant (8.314 J mol^{-1} K^{-1}).

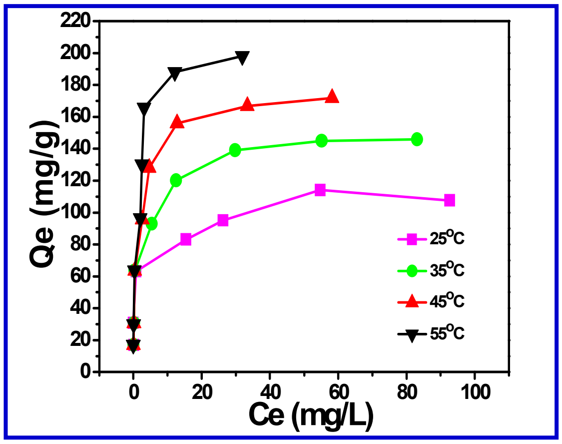

Fig. 9. Effect of uranium concentration on the adsorption of uranium by Fe_3O_4@SiO_2@Ni-L. (Adsorption dosage 0.05 g, reaction time 300 min, T = 25 ~ 55 °C and pH = 5)

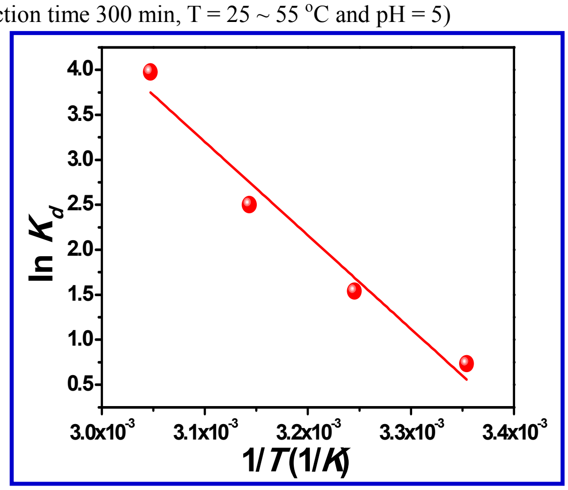

Fig. 10. Van't Hoff plot for removal of uranium by Fe_3O_4@SiO_2@Ni-L

The obtained thermodynamic parameters from Eqs. (4) and (5) are presented in Table 2. The positive value of *ΔH*° confirms the endothermic nature of adsorption. One possible explanation to this positive enthalpy change is that uranium (VI) ions dissolve well in water and have to be denuded of their hydration sheaths to some extent before sorption on Fe_3O_4@SiO_2@Ni-L, and the endothermicity of the desolvation process overwhelms the exothermicity of uranium (VI) ions attachment to the surface of Fe_3O_4@SiO_2@Ni-L; all values of *ΔG*° are negative, which indicate the feasibility of the adsorption process and the spontaneous nature of adsorption.

The positive value of *ΔS*° suggests the affinity of Fe_3O_4@SiO_2@Ni-L toward uranium (VI) ions in aqueous solutions and may imply some structural changes of the sorbents. The value of *ΔG*° becomes more negative with the increase of temperature, indicating more efficient sorption at high temperature. The positive *ΔS*° and negative *ΔG*° values indicate the spontaneous process of uranium (VI) sorption on Fe_3O_4@SiO_2@Ni-L and the affinity of Fe_3O_4@SiO_2@Ni-L toward the uranium (VI) ions in aqueous solutions.

Table 2 Thermodynamic parameters for adsorption of uranium on Fe_3O_4@SiO_2@Ni-L.

Temp (ºC)	ΔG° (kJ/mol)	ΔH° (kJ/mol)	ΔS° (J/mol/K)
25	-1.38	86.48	294.69
35	-4.33		
45	-7.28		
55	-10.22		

Adsorption isotherms

Isotherms are the equilibrium relations between the adsorbate concentrations in the solid and liquid phases. Maximum adsorption capacity is obtained from isotherms. The equilibrium adsorption data were analyzed by the well-known Langmuir and Freundlich isothermmodels.[38-39]

The Langmuir model considers several assumptions, such as localized adsorption, similar energies on all the active sites of the surface where no interaction between the adsorbed molecules occurs, and the surface of the heterogeneous catalytic reactions. Its linearized form can be expressed by the flowing equation:

$$C_e / q_e = 1/b \cdot q_m + C_e / q_m \quad (6)$$

where q_e (mg g^{-1}) is the amount of solution adsorbed per unit mass of adsorbent, C_e (mg L^{-1}) is the solute equilibrium concentration, q_m (mg g^{-1}) is the maximum adsorbate amount that forms a complete monolayer on the surface, and b (L mg^{-1}) is the Langmuir constant related to adsorption heat. When C_e/q_e is plotted against C_e and the data are regressed linearly, q_m and b constants are calculated from the slope and the intercept.

The Freundlich isotherm is an empirical equation assuming that the adsorption process takes place on heterogeneous surfaces, and adsorption capacity is related to the concentration of the adsorbate at equilibrium. The equation is commonly represented by:

$$\ln q_e = \ln K_f + n \ln C_e \quad (7)$$

K_f and n are the Freundlich constants related to the sorption capacity and sorption intensity, respectively.

The linear plots of Langmuir, Freundlich equations representing uranium (VI) sorption are illustrated in Fig. 11. The corresponding Langmuir, Freundlich parameters, along with the correlation coefficients, are reported in Table 3. As shown in Fig. 11A, the Langmuir equation fits the experimental data better than the Freundlich model with a higher correlation coefficient (R^2) of 0.99. The Langmuir model indicates that uranium (VI) absorbed form a monolayer coverage and chemisorption is the predominant sorption mechanism, which is consistent with the strong adsorption between uranium (VI) ions and Fe_3O_4@SiO_2@Ni-L functional groups. The maximum adsorption capacity of Fe_3O_4@SiO_2@Ni-L is evaluated as 110.3 mg U/g at 25 °C.

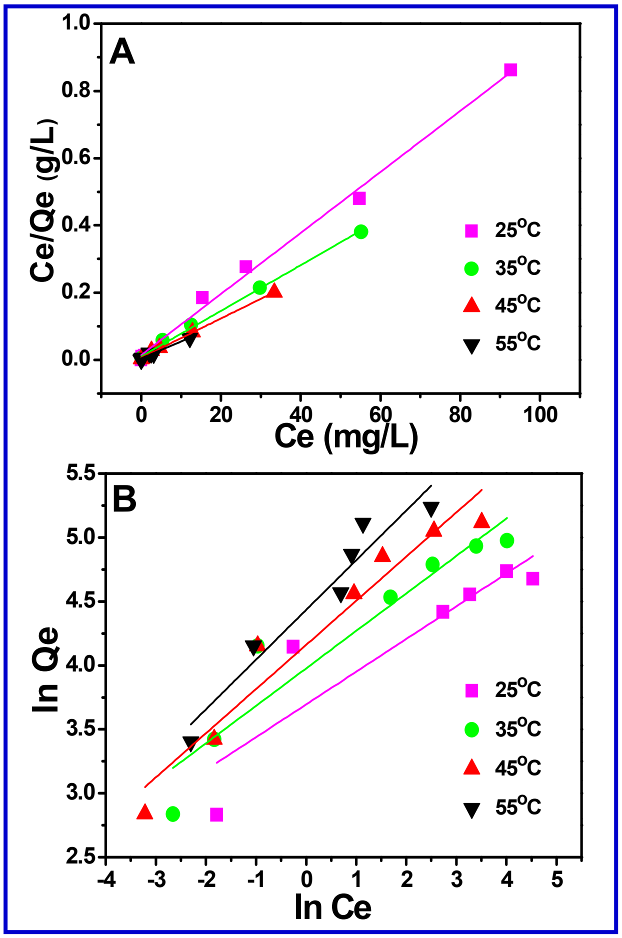

Fig. 11. Langmuir and Freundlich isotherm for removal of uranium by Fe_3O_4@SiO_2@Ni-L.

Table 3 Langmuir and Freundlich isotherm parameters for adsorption of uranium on Fe_3O_4@SiO_2@Ni-L

Temp	Freundlich			Langmuir		
(°C)	K_f	n	R^2	b	q_m (mg U/g)	R^2
25	40.2	0.26	0.77	0.623	110.3	0.99
35	53.4	0.29	0.89	0.686	147.3	0.99
45	64.1	0.35	0.93	0.944	170.9	0.99
55	84.3	0.39	0.92	1.188	197.6	0.97

Desorption and reusability study

Reusability is an important process in sorption studies due to it enhancing efficiency of use. Therefore, the reusability of Fe_3O_4@SiO_2@Ni-L was investigated to evaluate its application potential in removal and recovery of uranium (VI). As illustrated in Table 4, the Fe_3O_4@SiO_2@Ni-L shows a lower desorption yield using NaOH, Na_2SO_4, and water compared to $NaHCO_3$ solutions. 0.1 mol L^{-1} $NaHCO_3$ (88%) represents a high desorption yield for uranium. Hence, desorption tests showed that uranium is quantitatively desorbed with $NaHCO_3$.

To evaluate the regeneration of the adsorbent the adsorption/desorption cycle was repeated three times with the same adsorbent using 0.1 mol L^{-1} $NaHCO_3$ as desorbing agent. After three cycles, the sorption capacity of the Fe_3O_4@SiO_2@Ni-L decreases from 128.1 mg U/g to 99.6 mg U/g. This results show that the Fe_3O_4@SiO_2@Ni-L can be recycled. After three times circulation, the adsorption quantity only has a slight influence.

Table 4 Desorption yields of some desorptive solutions.

	Desorption solvent	Concentration (mol·L^{-1})	Desorption efficiency (%)
1	H_2O		6.35
2	Na_2EDTA	0.1	55.3
3	NaOH	0.1	46.8
4	Na_2SO_4	0.1	3.4
5	Na_2CO_3	0.1	51.2
6	$NaHCO_3$	0.1	88

Comparison of adsorbent performance with literature data

The removal of uranium (VI) by different adsorbents has been studied extensively. Table 5 represents the comparison of the adsorption capacity of uranium (VI) with other materials.[40-45] Adsorption capacity of Fe_3O_4@SiO_2@Ni-L equal to 129.26 mg U/g is higher than that of other adsorbents, except for MOFs. This data suggests that the Fe_3O_4@SiO_2@Ni-L as adsorbent is suitable for the removal of uranium (VI) from aqueous solution.

Table 5 Comparison of the uranium (VI) sorption capacity of Fe_3O_4@SiO_2@Ni-L with other sorbents.

Sorbents	Capacity (mg U/g)	Ref
Fe_3O_4/graphene oxide	69.5	40
Functionalized polymer-coated silica	5.2	41
Amine modified silica gel	21.4	42
Amidoxime modified Fe_3O_4@SiO_2	105.5	43
Oxime-grafted CMK-5	62	44
MOFs	217	45
Fe_3O_4@SiO_2@Ni-L	129.26	Present work

Removal Mechanism

The adsorption capacity of Fe_3O_4@SiO_2@Ni-L for uranium (VI) is 129.26 mg g^{-1} in this study, which is higher than most of the previously reported values of other materials. The adsorption mechanism is carried out in two steps; first, the presence of functional groups (such as -OH and -COOH) on the surface of

$Fe_3O_4@SiO_2@Ni$-L assures the capture of metallic cations (UO_2^{2+}) by surface complexation mechanisms. Second, UO_2^{2+} was strongly adsorbed as an inner-sphere complexes by means of surface complexation with Ni-O bond.[46-48] It could be concluded that the UO_2^{2+} is specifically adsorbed on the Ni-L loaded $Fe_3O_4@SiO_2$ through an inner-sphere complex via surface complexation rather than the electrostatic interaction.[49] Further studies are needed to more precisely characterize the detailed adsorption mechanism.

Conclusions

In the present study, a novel adsorbent, namely, $Fe_3O_4@SiO_2@Ni$-L was synthesized by chemically grafting Ni-L onto $Fe_3O_4@SiO_2$. It was characterized by various techniques: XRD、SEM、TEM、VSM and BET. Its efficiency in the separation and recovery of uranium (VI) was tested by batch technique. The maximum adsorption capacity for uranium was estimated to be 129.26 mg U/g, and the optimum conditions were found at pH 5.0 and 300 min contact time. Thermodynamic data suggested that the sorption of uranium (VI) onto $Fe_3O_4@SiO_2@Ni$-L was a spontaneous and endothermic process. In addition, uranium (VI)-loaded $Fe_3O_4@SiO_2@Ni$-L easily separated from aqueous solutions by a magnet and is efficiently renewed by $NaHCO_3$. The easy operation and efficient sorption performance indicated that $Fe_3O_4@SiO_2@Ni$-L can be used as a promising and powerful sorbent for the efficient removal of uranium (VI) from aqueous solutions.

Acknowledgment

This work was supported by National Natural Science Foundation of China (21353003), Special Innovation Talents of Harbin Science and Technology (2013RFQXJ145), Fundamental Research Funds of the Central University (HEUCFZ), Innovation Talents of Harbin Science and Technology (2014RFQXJ035), Natural Science Foundation of Heilongjiang Province (E201329), Natural Science Foundation of Heilongjiang Province (B201316), Program of International S&T Cooperation special project (2013DFR50060), and the fund for Transformation of Scientific and Technological Achievements of Harbin (2013DB4BG011), Research and Development of Industrial Technology Project of Jilin Province (JF2012C022-4).

Notes and references

[a] *Key Laboratory of Superlight Material and Surface Technology, Ministry of Education, Harbin Engineering University, Harbin 150001, China. Fax: +86 451 8253 3026; Tel: +86 451 8253 3026; E-mail address: zhqw1888@sohu.com*
[b] *Institute of Advanced Marine Materials, Harbin Engineering University, 150001, China.*
[c] *State Key Laboratory of Theoretical and Computational Chemistry, Institute of Theoretical Chemistry, Jilin University, Changchun 130023, China.*
[d] *Department of Chemical Engineering, Chengde Petroleum College, 067000, China.*

1 T.S. Anirudhan, C.D. Bringle, S. Rijith, J. Environ. Radioact. 2010, **101**, 267–276.
2 T.S. Anirudhan, L. Divya, P.S. Suchithra, J. Environ. Manage. 2009, **90**, 549–560.
3 W. Chen, W. Lu, Y. Yao, M. Xu, Environ. Sci. Technol. 2007, **41**, 6240–6245.
4 P. Pandit, S. Basu, Environ. Sci. Technol. 2004, **38**, 2435–2442.
5 R.F. Yunus, Y.M. Zheng, G.N.K. Nanayakkara, J.P. Chen, Ind. Eng. Chem. Res. 2009, **48**, 7466–7473.
6 X.M. Zhao, B.H. Zhang, K.L. Ai, G. Zhang, L.Y. Cao, X.J. Liu, H.M. Sun, H.S. Wang, L.H. Lu,. J. Mater. Chem. 2009, **19**, 5547–5553.
7 M. Asadullah, M. Asaduzzaman, M.S. Kabir, M.G. Mostofa, T. Miyazawa, J. Hazard. Mater. 2010, **174**, 437–443.
8 D. T. Hobbs, T. B. Peters, K. M. L. Taylor-Pashow and S. D. Fink, Sep. Sci. Technol., 2010, **46**, 119.
9 K. M. L. Taylor-Pashow, D. M. Missimer, A. Jurgensen and D. T. Hobbs, Sep. Sci. Technol., 2011, **46**, 1087.
10 V.S.R. Channu, R. Holze, B. Rambabu, Colloids and Surfaces A 2012, **414**, 204–208.
11 K. Anandan, V. Rajendran, Materials Science in Semiconductor Processing. 2011, **14**, 43–47.
12 B. Liu, H. Yang, H. Zhao, L. An, L. Zhang, R. Shi, L. Wang, L. Bao, Y. Chen, Sensors and Actuators B. 2011, **156**, 251–262.
13 Y. Zhang, Y. Gui, X. Wu, H. Feng, A. Zhang, L. Wang, T. Xia, International Journal of Hydrogen Energy. 2009, **34**, 2467–2470.
14 A. Bandara, J. Kubota, A. Wada, K. Domen, C. Hirose, Journal of Physical Chemistry B 1997, **101**, 361–368.
15 Y. Wang, Q.S. Zhu, H.G. Zhang, Chem. Commun. 2005, 5231–5233
16 L.X. Yang, Y.J. Zhu, H. Tong, Z.H. Liang, and W.W. Wang, Crystal Growth & Design. 2007, **7**, 2717-2719
17 A.A. Elabd , W.I. Zidan, M.M. Abo-Aly, E. Bakier, M.S. Attia, Journal of Environmental Radioactivity. 2014, **134**, 99-108
18 S.W. Zhang, J.X. Li, T. Wen, J.Z. Xu, X.K. Wang. *RSC Adv.*, 2013, **3**, 2754.
19 Y.M. Zhai, J.F. Zhai, M. Zhou, S.J. Dong, J. Mater. Chem. 2009, **19**, 7030–7035.
20 A. Bhatnagar, A.K. Jain, J. Colloid Interface Sci. 2005, **28**, 49–55
21 Y.C. Chang, D.H. Chen, J. Colloid Interface Sci. 2005, **283**, 446–451
22 S. H. Xuan, Y. X. J. Wang, J. C. Yu and K. C. F. Leung, *Langmuir*, 2009, **25**, 11835.
23 Y.H. Deng, C.C. Wang, J.H. Hu, W.L. Yang, S.K. Fu, Colloids Surf., A. 2005, **262**, 87.
24 U. Kalapathy, A. Proctor, J. Shultz, Bioresour. Technol. 2000 **73** 257–262.
25 M. Das, S. Chatterjee, S. Chattopadhyay, Polyhedron 2014 **68** 205–211.
26 L. Xiang, X.Y. Deng, Y. Jin, Scripta Materialia 2002 **47** 219–224.
27 P.D.C. Dietzel, B. Panella, M. Hirscher, R. Blom and H. Fjellvag, Chem. Commun. 2006 **959** 959–961.
28 S. Sadeghi, H. Azhdari, H. Arabi, A.Z. Moghaddam, J.

Hazard. Mater. 2012, **215**, 208–216
29 B. Cheng, Y. Le, W.Q. Cai, J.G. Yu, J. Hazard. Mater.2011, **185**, 889.
30 J.G. Yu, Y.R. Su, B Cheng, Adv. Funct. Mater.2007, **17**, 1984.
31 X.X. Yu, J.G. Yu, B. Cheng, M. Jaroniec, J. Phys. Chem. C 2009, **113**, 17527.
32 A. Schierz, H. Zaker, Environ. Pollut. 2009, **157**, 1088-1094.
33 G. Wang, J. Liu, X. Wang, Z. Xie, N. Deng, J. Hazard. Mater. 2009, **168**, 1053-1058.
34 Y.S. Ho, G. McKay, Water Res. 2000, **34**, 735–742.
35 Y.S. Ho, J. Hazard.Mater. 2006, **136**, 681–689.
36 A.K. Bhattacharyal, T.K. Naiya, S.N. Mondal, S.K. Das, Chem. Eng. J. 2008, **137**, 529–541
37 L.M. Zhou, J.Y. Jin, Z.R. Liu, X.Z. Liang, C. Shang, J Hazard Mater. 2011, **185**, 1045–1052
38 N. Sharma, K. Kaur, S. Kaur, J. Hazard. Mater. 2009, **163**, 1338–1344.
39 A. Bhatnagar, A.K. Jain, J. Colloid Interface Sci. 2005, **28**, 49–55.
40 P.F. Zong, S.F. Wang, Y.L. Zhao, H. Wang, H. Pan, C.H. He, Chem. Eng. J. 2013, **220**, 45–52
41 D.E. Bryant, D.I. Stewart, T.P. Kee, C.S. Barton, Environ. Sci. Technol. 2003, **37**, 4011–4016
42 K.A. Venkatesan, V. Sukumaran, M.P. Antony, P.R.V. Rao, J. Radioanal. Nucl. Chem. 2004, **260**, 443–450
43 Y.G. Zhao, J.X. Li, L.P. Zhao, S.W. Zhang, Y.S. Huang, X.L. Wu, X.K. Wang, Chem. Eng. J. 2014, **235**, 275–283
44 G. Tian, J.X. Geng, Y.D. Jin, C.L. Wang, S.Q. Li, Z. Chen, H. Wang, Y.S. Zhao, S.J. Li, J. Hazard. Mater. 2011, **190**, 442–450
45 M. Carboni, C.W. Abney, S.B. Liu and W.B. Lin, Chemical Science. 2013, **4**, 2396
46 J. Roques, E. Veilly, E. Simoni, Int. J. Mol. Sci. 2009, **10**, 2633-2661
47 P.J. Pretorius, P.W. Linder, Appl. Geochem. 2001,**16**, 1067-1082
48 Y. Xu, T. Boonfueng, L. Axea, J. Colloid. Interf. Sci. 2006,**299**, 28-40
49 A. Predescu, A. Nicolae, U.P.B. Sci. Bull. 2012,**74**, 255-264